Inorganic Chemistry Communications 149 (2023) 110387

Contents lists available at ScienceDirect

Inorganic Chemistry Communications

journal homepage: www.elsevier.com/locate/inoche

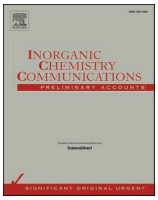

Short communication

An expedient synthesis of C3-arylidene-oxindole derivatives using calcite nanoflowers as an efficient heterogeneous catalyst

Dnyaneshwar Sanap [a,b,*], Lata Avhad [c], Suresh Ghotekar [d,*], Nitin D. Gaikwad [a,*]

[a] Department of Chemistry, Organic Chemistry Research Centre, K.R.T. Arts, B.H. Commerce, and A.M. Science College, Gangapur Road, Nashik 422 002, Savitribai Phule Pune University, Maharashtra, India
[b] Department of Chemistry, Organic Chemistry Research Centre, G.M.D. Arts B.W. Commerce and Science College, Sinnar 422 103, Savitribai Phule Pune University, Maharashtra, India
[c] Department of Chemistry, Arts, Commerce and Science College Dindori, Nashik 422 202, Savitribai Phule Pune University, Maharashtra, India
[d] Department of Chemistry, Smt. Devkiba Mohansinhji Chauhan College of Commerce & Science (University of Mumbai), Silvassa 396 230, Dadra and Nagar Haveli (UT), India

ARTICLE INFO

Keywords:
$CaCO_3$ nanoflowers
C3-arylidene-2-oxindole
Knoevenagel condensation

ABSTRACT

α-β unsaturated heterocyclic compounds such as C3-arylidene-oxindoles, with five-member rings containing nitrogen, have an important role in the realm of medicine. This study aims to synthesize the C3-arylindene-oxindoles derivative compounds using calcite nanoflowers ($CaCO_3$ NFs) as a heterogeneous catalyst for the first time. These $CaCO_3$ NFs prepared by the thermal decomposition method, which is an active and reusable catalyst for stereospecific Knoevenagel condensation reaction between 2-oxindole and aromatic aldehyde under different solvent conditions like water, ethyl alcohol, and 50 % aqueous ethyl alcohol. This catalytic method is employed with a wide range of aromatic aldehydes to produce high yields of C3-arylidene-oxindoles (93–99 %), with stereo-specifically *E*-isomers (100 %) for 50 % alcohol and alcohol as a solvent.

1. Introduction

Oxindole is a unique scaffold for constructing and creating biologically important medicines and agents by changing the substituent. The oxindoles and their derivative framework are often considered a privileged heterocycle found in medicinally useful natural and synthetic scaffolds. Moreover, it was first found in the *Uncaria tomentosa* plant, commonly known as cat claw's plat, which was found abundantly in the Amazon rainforest [1,2]. Oxindole and its derivative scaffold have a diverse range of pharmacological activities [3]. C3-arylidene [4], C3-spiro [5,6], and chiral C3-disubstituted [7,8] oxindoles have immense medicinal use. In this particular, C3-arylidene-oxindole derivatives are medicinally important and exist in a wide range of activities: kinase inhibitor [9–16], antitumor activity [17–20], anti-inflammatory [21], antiproliferative activity [22], antiproliferative and antiviral properties against SARS-CoV-2 [23], neuroprotective [24], Alzheimer's disease [25], anti-plasmodial agents [26], anti-depressive agents [27], and inhibitors of *Plasmodium falciparum* cyclin-dependent protein kinases [28]. Moreover, 3-arylidene-oxindoles are also well-known prochiral electrophiles and represent a broadly successful strategy for the synthesis of biologically active chiral Spiro-oxindoles [29–39] and natural product TMC-95-A and B [40], gelsemine [41]. Spiro oxindole is a potent inhibitor for HIV replication [42,43], anticancer agents [44–46], and a broad spectrum of other activity [47,48].

Conventionally, 3-arylidene-oxindoles (Yield: 10–88 %) were synthesized by Knoevenagel condensation between oxindole and aromatic carbaldehyde assisted by secondary or tertiary amine bases under polar solvents conditions [22,49,50]. Hongming Jin et al. report the dehydrogenative 3-alkenylation (Yield: 30–83 %) of N-substituted oxindole with benzylic alcohols catalyzed by a homogenous rhenium hetaphydride complex [51]. Girish Singh Bisht et al. [52] demonstrate the dehydrogenative coupling of diarylmethanols with 2-oxindole to the synthesis of 3-(diphenylmethylene) indolin-2-one using Ru(II)–NHC catalyst in the absence of acceptor in good yield 31–87 %. Cedric Van Goethem et al. [53] demonstrated the synthesis of 3-benzylidene-oxindole by coupling the oxindole with benzaldehyde on Zr-incorporated UiO-66 metal–organic framework (MOF) as a catalyst. However, these conventional catalytic approaches work with activated (aromatic and

* Corresponding authors at: Department of Chemistry, Organic Chemistry Research Centre, K.R.T. Arts, B.H. Commerce, and A.M. Science College, Gangapur Road, Nashik 422 002, Savitribai Phule Pune University, Maharashtra, India (D. Sanap).
E-mail addresses: sanapdnyanu90258@gmail.com (D. Sanap), ghotekarsuresh7@gmail.com (S. Ghotekar), gaikwad_nd17@yahoo.co.in (N.D. Gaikwad).

https://doi.org/10.1016/j.inoche.2022.110387
Received 17 July 2022; Received in revised form 16 December 2022; Accepted 30 December 2022
Available online 2 January 2023

allylic) aldehydes. However, they suffer from low yields of products, harsh reaction conditions, and problems with catalyst recycling and reusability, respectively. Lipase-biocatalytic [54] Knoevenagel condensation was reported to promote the synthesis of benzylidene-indolin-2-ones (Yield: 75–96 %) between 1,3-dihydroindol-2-one and aromatic aldehydes. The synthesis of 3-arylidene-1,3-dihydroindol-2-ones (Yield: 86–97 %) catalyzed by a Bronsted acidic ionic liquid (1-(3-sulfonic acid) propyl-3-methylimidazolium hydrogen sulfate) [55] was reported between oxindole and aromatic aldehyde. The major drawback of using Lipase and Bronsted acidic ionic liquid catalysts for 3-arylidene-oxindoles synthesis is the excess amount of catalyst and the typical recycling process and reusability of catalyst. Didier Villemin et al. [56] investigate the dry condition 3-alkenylation of oxindole with a ketone (Yield: 36–76 %) and aromatic aldehyde (Yield: 69–94 %) using alumina-supported potassium fluoride ($KF\text{-}Al_2O_3$) in the presence of microwave radiation. Hyun Ju Lee et al. [57] reported the selective synthesis of (*Z*)-3-arylidene-oxindoles (Yield: *Z:E*, 3 %:90 % to 85 %:9 %) using a mixture of $Ti(O^iPr)_4$/Pyridine with unsymmetrical ketones. Parisa Gholamzadeh et al. developed the synthesis of *trans*-isoindigo derivatives (Yield: 40–90 %) [58] and (*E*)-arylidene-1,3-dihydroindole-2-ones (Yield: 40–90 %) [59] with isatin, activated aromatic aldehyde respectively, using reusable heterogeneous SO_3H-loaded silica catalyst (SBA-Pr-SO_3H) under solvent-free conditions. In 2020, Md. Nurnobi Rashed et al. [60] investigated (*E*)–C3-selective alkenylation of oxindole (Isolable yield: 87–99 %, and 79–93 % to *E*-isomers stereo-selectively) using aldehydes and commercially available CeO_2 was employed as a heterogeneous active and reusable catalyst, under solvent-free conditions (Scheme 1**a**).

Generally, carbonate anions act as a strong base capable of deprotonating the active methylene compounds, with the consequent formation of a carbanion stabilized via the coordination with calcium cation, which combines with a carbonyl compound, eventually leading to the Knoevenagel product. Hence, there is no special requirement for an additional base for the deprotonation. Therefore, calcite simultaneously plays a dual role as a base and catalyst. As a result, the choice of calcite as a catalyst for Knoevenagel condensation is more advantageous than other metal catalysts. However, there are six major challenges embedded in this reaction: 1) harsh reaction conditions; 2) long reaction time; 3) elevated temperature; 4) use of hazardous solvent; 5) low to moderate yield; 6) low stereo-selectivity in product formation. Herein, we report this strategy's successful implementation for synthesizing 3-arylidene-oxindoles in the 93–98 % yield (Scheme 1**b**), with high stereo-specifically *E*-isomer (Yield: ~100 %). The structure of the product was confirmed by ^1H NMR, ^{13}C NMR, and HR-MS.

2. Experimental

2.1. Chemical/materials

Calcium nitrate tetrahydrate, sodium hydroxide, ethylene glycol, 2-oxindole, substituted aromatic aldehydes, ethyl alcohol, acetone, acetonitrile, dichloro methane (DCM), 1, 4-dioxane, ethyl acetate, n-hexane, methyl alcohol, trichloromethane, dimethyl sulfoxide (DMSO), and dimethylformamide (DMF) were procured from S. D. Fine Chem Limited. All of the solvents used in this study were purified before they were used.

2.2. Characterization techniques

A UV–visible diffuse reflectance spectrum (UV-DRS) of NFs was obtained by Jasco Spectrophotometer model V-770. The absorption spectra were recorded in the range of 200 nm to 800 nm. Fourier transform infrared (FT-IR) spectra of NFs were obtained using a JASCO-4600-Type-A Spectrophotometer, set in the range of 400 to 4000 cm^{-1}. X-ray Diffraction (XRD) of milled powder was performed using a Bruker D8 Advance Diffractometer (40 kV and 35 mA) with Cu-Kα radiation (λ = 1.54060 A^0) to analyze the crystal structure. The XRD lower-angle measurement for NFs is 20^0 to 80^0 with a minimum step size (2θ) of 0.020^0. The cross-section morphology of NFs was examined using field-emission scanning electron microscopy (FE-SEM). The surface structure was visualized using the FE-SEM, FEI Nova Nano SEM 450 instrument at an accelerating voltage of 10 kV. The high-resolution transmission electron microscopy (HR-TEM) images were obtained using a JEOL (JEM-2100) instrument equipped with a LaB6 electron gun with an accelerating voltage of 200 kV. The N_2 adsorption–desorption data were obtained at 77 K in a NOVA 1000e (Quanta-chrome Instruments), and the surface area was calculated using the Brunauer-Emmett-Teller (BET) equation. The Barret, Joyner, and Halenda (BJH) pore diameter method was achieved from the materials desorption branch of the isotherm. The zeta potential of NFs was determined using HORIBA SZ-100 (Z Type Version 2.00) instrument, using water as a dispersive medium. CO_2-temperature-programmed desorption (CO_2-TPD) was carried out using

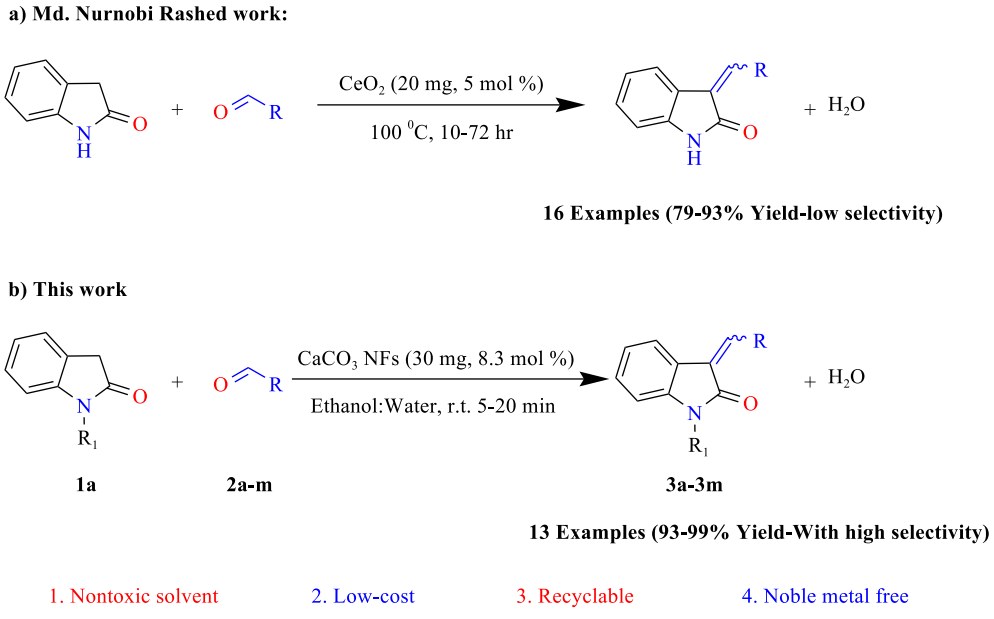

Scheme 1. Strategies for the construction of 3-arylidene-oxindoles.

BELCAT-II instrument having 0.5.1.10 Version, with the loading of 86 mg of the sample at 300 °C for 90 min, with a constant stream of He gas (flow rate: 50 SCCM) for pre-treatment; it results in removal of adsorbed water and carbonates associated with the catalyst surface. After cooling to 50 °C, pure He-airstream was introduced into the reactor (pre-treated sample) and kept flowing for 16 min after cleaning treatment; the CO_2 was switched into the reactor and kept for the next 30 min at 50 °C. All thermal treatments were carried out with a heating rate of 10 °C min^{-1} and the MFC total flow rate of 30 SCCM. The TPD experiments were performed in the range of 50 °C to 800 °C in the presence of Helium-gas flow.

Catalytic synthesis of C3-arylidene-2-oxindole was confirmed by Nuclear Magnetic Resonance (NMR) analysis by recording the spectra at 500 MHz (^{1}H) and 126 MHz (^{13}C) using Bruker Advance NEO 500 MHz Spectrometer. The molar mass and fragmentation pattern of synthesized organic compounds were recorded over the range of *m/z* 50 to 800 using Bruker Impact HD HR-MS instrument. The melting points of synthesized C3-arylidene-2-oxindole were determined using Thiele's tube assembly and are uncorrected.

2.3. Synthesis of Calcite nanoflowers

The synthesis of Calcite nanoflowers by the thermal decomposition method has four consecutive basic processes (Scheme 2). In this experiment, a homogeneous solution of $Ca(NO_3)_2$ salt (the precursor) was produced by dissolving the 3 gm of $Ca(NO_3)_2{\cdot}4H_2O$ in 15 mL of ethylene glycol (the capping agent and solvent). On the other hand, the homogeneous solution of NaOH was prepared by dissolving the 1.35 gm of NaOH (the precipitant) into 5 mL of ethylene glycol. The next step was adding NaOH solution (drop by drop) to the homogenous salt solution with constant stirring at 700 to 800 RPM for the next 30 min at ambient temperature. After the addition of sodium hydroxide solution, the mixture was stirred for the next 2 h and kept steady for the next 10 h at ambient temperature to get gel formation. Further, the slow addition of deionized water resulted in a low nucleation rate and encouraged subsequent precipitation of $Ca(OH)_2$ one over another, forming a highly crystalline gel. Then filtration was followed, where the filtrate was cleaned with deionized water to remove adsorbed impurities and soluble salt associated with the precipitate. The synthesizing process was ended by drying the precipitate at 70 °C for 3 h in a hot air oven and calcinating at 400 °C for 3 h in the muffle furnace, with a heating rate of 5 °C for 2 min till achieving a temperature of 400 °C for calcination. After cooling

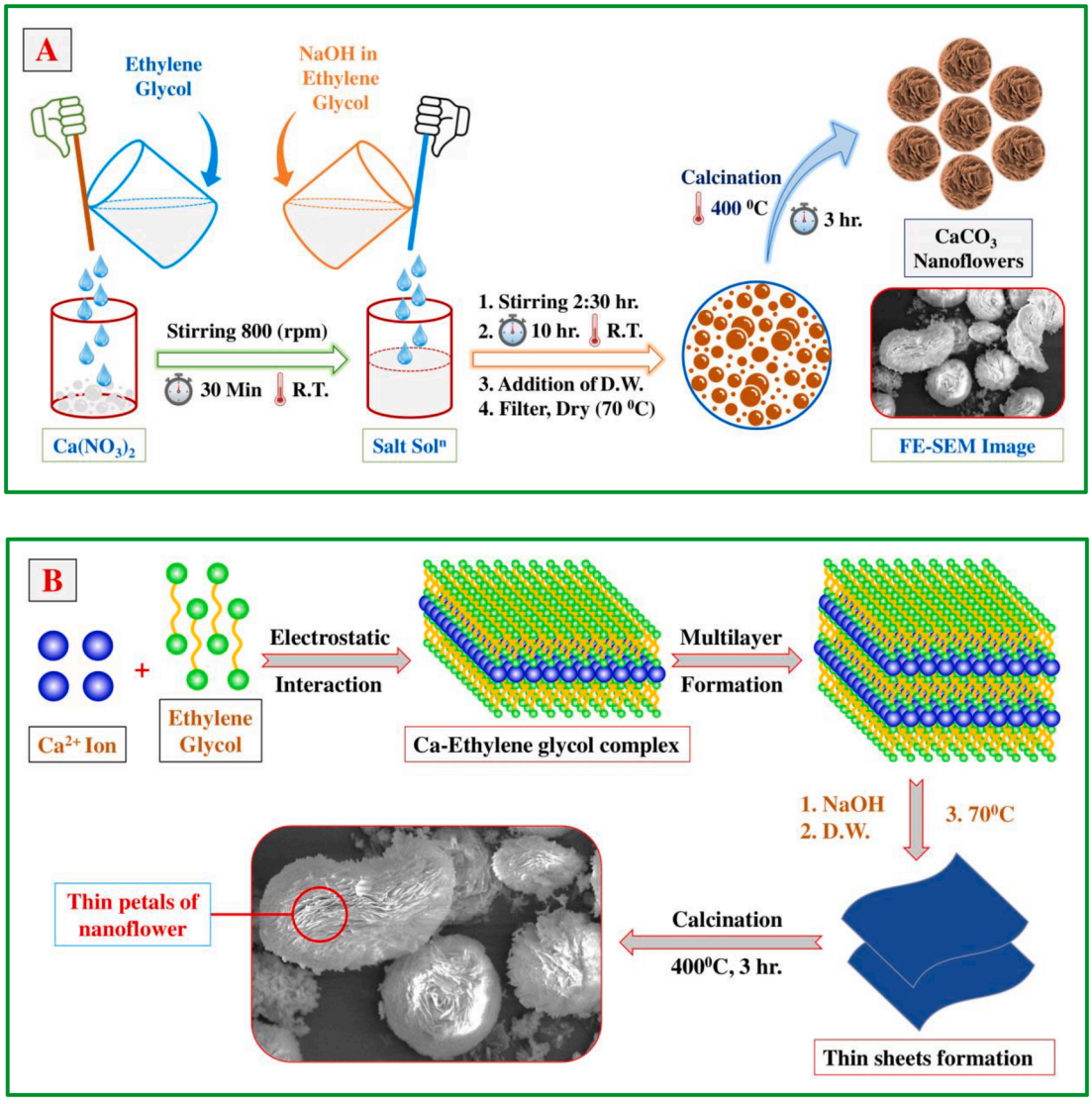

Scheme 2. Formation of $CaCO_3$ nanoflowers (NFs) (A) Schematic diagram describing the synthesis of Calcite nanoflower, (B) Schematic illustration for the formation of flower petals.

to room temperature, the harvested $CaCO_3$ NFs were ground and stored in a sealed glass vial to examine the catalytic activity in the Knoevenagel condensation reaction.

2.4. General procedure for coupling

In a 25 mL round bottom flask, a mixture of 2-oxindole (1.5 mmol), aromatic aldehyde (1.8 mmol), and $CaCO_3$ NFs (0.3 mmol) was well stirred (200 RPM) in the presence of 2 mL 50 % ethanol (mixture of 1 mL distilled water and 1 mL ethanol) (Table 4, Entry 1 to 13) at room temperature. The progress of the reaction was monitored by a thin layer of chromatography (n-hexane and ethyl acetate, 1:1 proportion). After the end of the reaction, the reaction mixture is added to a separating funnel that contains ethyl acetate (15 mL); shake it well, remove the bottom aqueous layer and filter the organic layer using simple filtration. $CaCO_3$ NFs on filter paper were subsequently washed with ethyl acetate (5 mL), dried, and used for a consecutive cycle. Further product purification was done by silica column chromatography (60–120 mesh size of silica) using n-hexane: ethyl acetate (with proportion 95:5 to 70:30) to give the corresponding product in the pure form. Following the completion of the reaction, an aqueous extractive workup and column chromatographic purification produced the (*E*)-isomer of C3-arylidene-2-oxindole as the main product. All organic products are confirmed by ^{1}H NMR, ^{13}C NMR, and HR-MS techniques.

2.5. Physical, chemical, and structural characterization of catalyst

The UV-DRS spectrum of synthesized $CaCO_3$ NFs (Fig. 1**a**) shows a broad absorption spectrum in the range of 205–335 nm. The absorption peak at 285 nm corresponds to the formation of the Calcite nanoparticles. Based on the Tauc plot, the band-gap energy estimated from the tangent intercept to the plots of αhϑ vs. energy is 3.96 eV by the direct method (Fig. 1**b**). This implies that the as-synthesized $CaCO_3$ NFs is a visible light active material. Therefore, the strong absorption band in this area is the outcome of ligand-to-metal charge transfer (LMCT) direct transition. The calculated band gaps of $CaCO_3$ NFs are in good agreement with the calculated band gap reported earlier by Aboutaleb et al. [61].

Fig. 2 shows Fourier transfer-infrared (FT-IR) spectra of $CaCO_3$ NFs. The strong and sharp band at 3643 cm^{-1} and broad band at 3425 cm^{-1} correspond to the free and hydrogen-bonded O—H stretching of bonds, respectively, from the remaining hydroxide [62–64] or from the water molecules (moisture), which are adsorbed on the surface of the samples during handling to record the spectra [65]. The typical sharp band at 1438 cm^{-1}, 874 cm^{-1}, and 712 cm^{-1} represents an asymmetric stretching, out-of-plane bending, and in-plane bending vibration for the carbonate ion group, respectively [66]. Besides the fundamental mode of vibration, the overtone band at 1795 cm^{-1} and 2514 cm^{-1} is observed due to the combination of [(874 cm^{-1}) + (712 cm^{-1})] bands [67].

The X-ray diffraction pattern of synthesized powder shows that the sample contains a significant amount of crystalline-trigonal (hexagonal axes) calcite ($CaCO_3$) phase. The X-Ray Diffraction pattern of the synthesized nanoflowers is illustrated in Fig. 3, and was indexed to (012), (104), (006), (110), (113), (202), (024), (018), (116), (211), (122), (1010), (214), (208), (119), (125), (300), (0012), (217), (0210), (128), (306), (220), and (1112) planes, characteristic to the hexagonal crystal structure of $CaCO_3$ (JCPDS No. 86-0174). All these planes correspond to the 2θ value of 23.10°, 29.43°, 31.44°, 36.03°, 39.42°, 43.20°, 47.16°, 47.52°, 48.54°, 56.58°, 57.45°, 58.11°, 60.69°, 60.81°, 61.35°, 63.15°, 64.68°, 65.61°, 69.21°, 70.20°, 72.93°, 73.71°, 76.29°, and 77.16°, respectively. The average crystallite size estimated by the Debye-Scherer equation using FWHM (Full Width at Half Maximum) of the most prominent (104) peak was found to be 47 nm, with the lattice parameter of 0.3 nm.

FE-SEM and HR-TEM characterization were used to determine the catalyst morphology. Fig. 4**a-c** possesses a nanoflower-like morphology

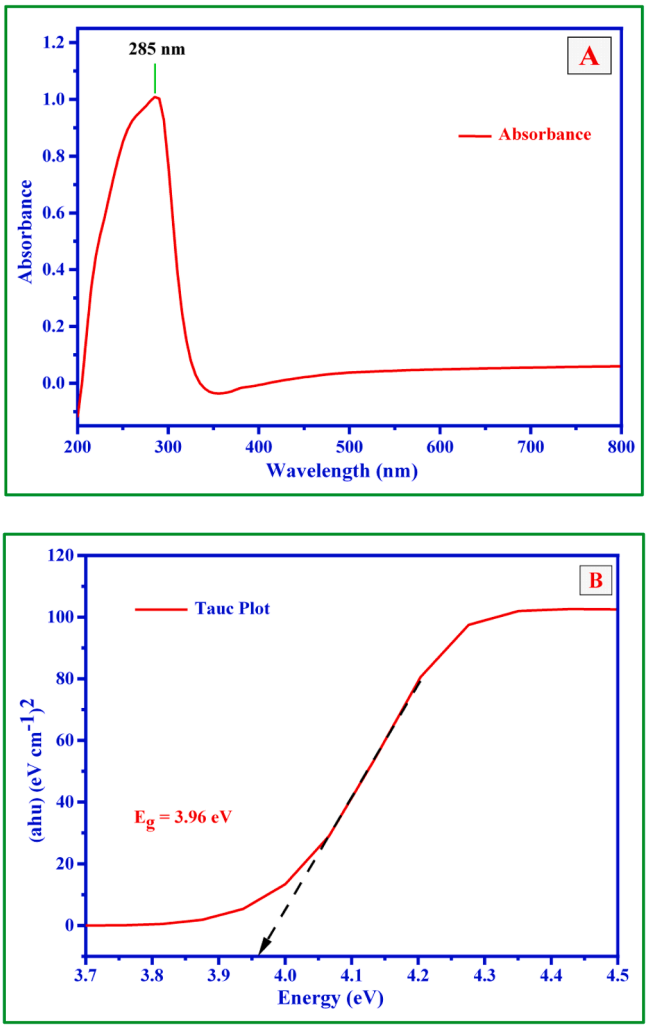

Fig. 1. a) UV-DRS spectrum of synthesized $CaCO_3$ nanoflower, b) band-gap energy by Tauc plot.

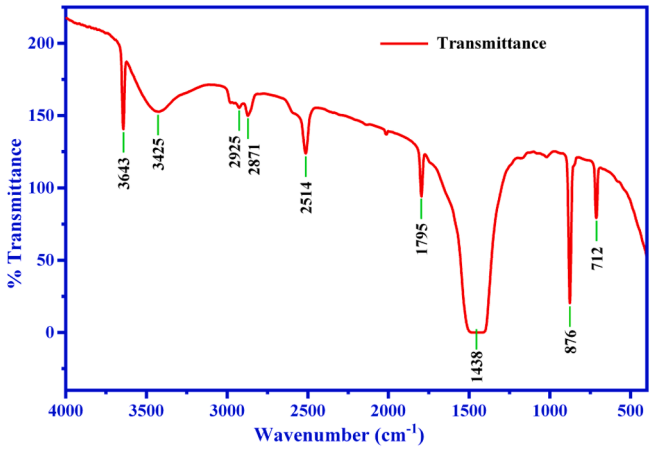

Fig. 2. FT-IR spectrum of synthesized $CaCO_3$ nanoflowers.

with a diameter of fewer than ~5 μm. The morphology of $CaCO_3$ NFs is observed as a marigold flower (as shown in Fig. 4**b**) with petals. However, we observed the highly porous and hollow structures having capsule-like (Fig. 4**d**), and hexagon (Fig. 4d) in FE-SEM images. Additionally, in Fig. 4d, the synthesized NFs exhibit a narrow particle size distribution in the range of 46–52 nm, with a mean diameter of ~49 nm

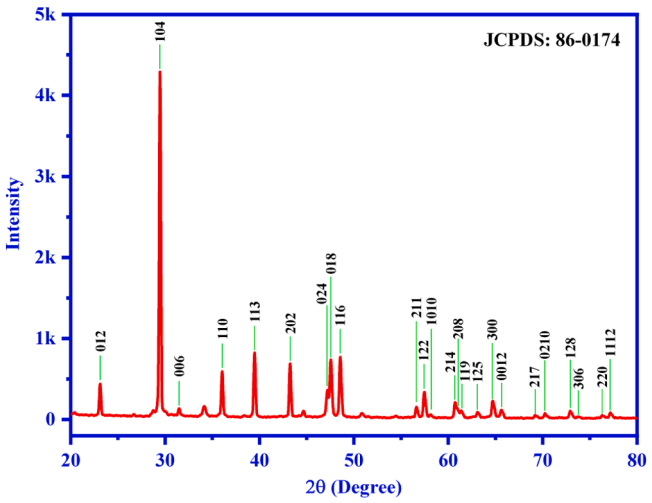

Fig. 3. XRD patterns of synthesized $CaCO_3$ NFs.

for $CaCO_3$ NFs.

The microcrystal structure of the material was further studied by HR-TEM (Fig. 5**a-f**). The well crystalline nanoparticles with the uniform grain size distribution having a diameter in the range of 35–57 nm and length of 35–101 nm have an average diameter of 49 nm and length of 84 nm for hexagons, respectively (Fig. 5**g-h**). The HR-TEM images (Fig. 5**d-e**) have clear lattice fringes with an interplanar spacing of ~0.3 nm and ~0.24 nm due to reflection from the (1 0 4) and (1 1 0) plane. The SAED pattern (Fig. 5**f**) shows high crystallinity in the nanostructure. These findings are well consistent with the XRD and FE-SEM analysis (Fig. 4d).

The 3-Dimensional flower-like microstructure of NFs exhibits large pore volumes and surface area, which is beneficial to reactant adsorption. The calcined catalyst's specific surface areas and porosity were measured by the nitrogen adsorption–desorption Brunauer-Emmet-Teller (BET) method to determine textural properties (Fig. 6). In our study, we calculate the data for surface areas and pore volume, and it can be observed that significantly higher external surface area (4.65 m^2 g^{-1}), mesopore volume (0.049 cm^3 g^{-1}), and pore diameter (43 nm) of synthesized NFs. It is noteworthy that the non-coincident shape of isotherms at the high relative pressure ($P/P_0 \geq 0.9$) revealed the presence of numerous micropores in the $CaCO_3$ NFs, which may be attributable to the voids of nano-$CaCO_3$ aggregates after template removal. This provided evidence that ethylene glycol was a functional auxiliary dispersion for preventing $CaCO_3$ NF aggregation, resulting in a small number of micropores in the $CaCO_3$ NFs.

The stability of the prepared $CaCO_3$ NFs was investigated using dynamic light scattering analysis, and the result is shown in Fig. 7. The mean zeta potential of synthesized NFs was found to be −3.3 mV. Previously, $CaCO_3$ had a reported zeta potential of roughly −10 mV [68], which suggests that the newly formed $CaCO_3$ clusters are inherently unstable. It is the cause of the micron-sized particles that were created when newly formed particles were aggregated. It was recognized that several factors, including surface modifiers, additives, and ions, had an impact on the surface potential of $CaCO_3$. For instance, the zeta potential of $CaCO_3$ was positive in solutions with high Ca^{++} ions and negative in those with excess CO_3^{2-} ions [69]. In order to produce stable $CaCO_3$ particles, it is crucial that additional ions, also known as the potential determining ions (PDI), such as crystal lattice ions, surface hydrolysis ions, and adsorbing ions in solution, are present.

CO_2-TPD analysis was carried out to determine the surface basicity of the materials. Commonly, it was believed that CO_2 adsorbed on weaker basic sites would be desorbed at lower temperatures and that adsorbed on stronger basic sites would be desorbed at higher temperatures. The CO_2-TPD profile of synthesized $CaCO_3$ NFs (Fig. 8) shows a strong and broad CO_2 desorption peak in the region of 370–558 °C. Especially, the intensities of the desorption peaks increased, and the vertices of the desorption peaks experienced a little migration toward higher temperatures from 370 °C to 535 °C. Therefore, based on the phenomena mentioned above, it could be speculated that the desorption peak around 370 °C to 558 °C might be derived from the weakly chemisorbed CO_2 and physically adsorbed CO_2 due to the large pore volumes and specific surface areas of synthesized NFs. However, the other desorption peak at 556 °C to 806 °C might be related to strong basic sites. The desorption peak around 780 °C might be caused by the desorption of strongly adsorbed CO_2 on the surface of calcite. Furthermore, it was believed that the high numbers of basic sites on the surface of the catalyst are available, which leads to high chemisorption of the CO_2, which had been confirmed by CO_2-TPD analysis. In general, it was sure that $CaCO_3$ NFs with high basic canters would affect the catalytic properties of the C3-arenylation of 2-oxindole with the aromatic aldehyde.

3. Result and discussion

3.1. Screening of reaction condition for the C3-arenylation of oxindole

We investigated several potential catalysts for the C3-arenylation of 2-oxindole (1a) with benzaldehyde (2a) into the corresponding 3-benzylidene-oxindole product (3a). We used a variety of potential catalysts to determine the best one to give 3a in the highest yield. At room temperature for 25 min, a variety of heterogeneous and homogeneous catalysts (10 mg) were used to investigate the C3-arenylation of 1a (1.5 mmol) with 2a (1.8 mmol). Table 1 summarises the yields of 3a for employing various potential catalysts.

In this experiment, we investigated the catalytic activity of several acidic, amphoteric, and basic catalysts and discovered that the reaction was not observed without a catalyst (Entry 1). Commercially available heterogeneous Lewis acidic oxide *K*10 Montmorillonite, basic oxide $CaCO_3$, $NaCO_3$, and homogeneous amphoteric calcium nitrate gave 5 %, 11 %, 5 %, and 4 % yield, respectively (Table 1, Entry 2–5). Heterogeneous amphoteric metal oxide, including ZnO and NiO, gave a low yield of 17 % and 15 %, respectively (Table 1, Entry 6–7), and basic metal oxide, including CuO, MgO and CaO, gave a moderate yield of 24 %, 37 % and 59 % respectively (Table 1, Entry 8–10). Among entries, 2 to 11, the heterogeneous Lewis basic oxide, including $CaCO_3$ NFs (Table 1, Entry 11) shows the highest yield of C3-benzylidene-oxindole 3a (74 %). The screening test in Table 1 shows that the most efficient catalyst for the C3-arenylation of 1a with 2a is $CaCO_3$ nanoflowers (Table 1, Entry 11).

We optimized the reaction conditions (mole fraction of benzaldehyde and solvent) for the model C3-arenylation process **(**Table 2, Entry 1-19**)** using Calcite nanoflower (10 mg, 0.1 mmol) as the potential catalyst for Knoevenagel condensation reaction. The percent yield of the C3-arenylation process depends on the molar amount of 2a and the solvent used for the reaction. C3-arenylation with 1.8 equivalent of 2a and a mixture of Water:Ethanol (1:1) combination gave the highest yield (74 %) within minimum time and ambient temperature (Table 2, Entry 11).

Under optimized conditions (1.5 mmol of 1a, 1.8 mmol 2a, and Water:Ethanol (1:1) solvent). We further screened the catalytic amount of $CaCO_3$ **(**Table 3**)** and found that 30 mg (0.3 mmol) of catalyst gave the highest yield of 3a (99 %) within 5 min. Regardless of the electronic nature of substrates with substituents at the *ortho*, *meta* or *para* position and specifically afford *E*-isomers **(**Table 4**)**. However, the diverse reports on the synthesis of 3-arylidene-oxindoles using various catalysts and their results are described in Table 5.

Spectral data of synthesized compounds are as follows:

(E)-3-benzylideneindolin-2-one (3a)

The title compound was obtained after silica (60–120 mesh) column chromatography (Hexane: Ethyl acetate: 85:15 to 40:60); Colour: Bright

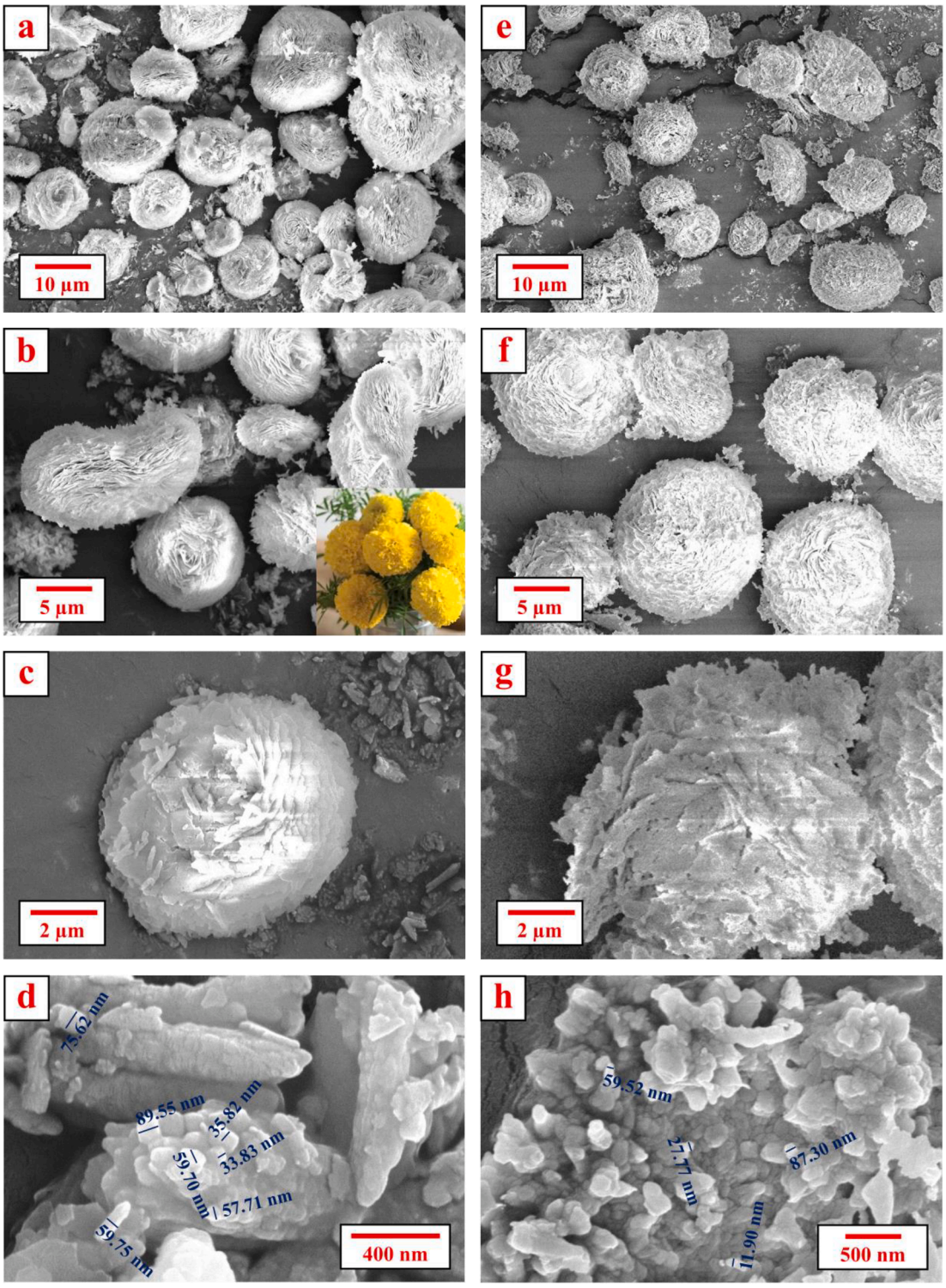

Fig. 4. FE-SEM images of flower-like Calcite microsphere for unused NPs (a-d), after reused for successive five cycles (e-h).

yellow needles; Yield: 99 %; MP: 175–176 °C; **^{1}H NMR** (500 MHz, $CDCl_3$) δ: 9.34 (s, 1H), 7.86 (s, 1H), 7.68 (d, J = 7.1 Hz, 2H), 7.64 (d, J = 7.7 Hz, 1H), 7.50–7.42 (m, 3H), 7.22 (t, J = 7.7 Hz, 1H), 6.95 (d, J = 7.7 Hz, 1H), 6.87 (t, J = 7.7 Hz, 1H); **^{13}C NMR** (126 MHz, $CDCl_3$) δ: 170.83, 141.96, 137.65, 134.99, 130.04, 129.79, 129.47*, 128.79*, 127.88, 123.13, 121.93, 121.81, 110.52; **HR-MS** for $C_{15}H_{12}NO$ $(M + H)^+$: 222.09, found: *m/z*: 222.09.

(E)-3-(4-fluorobenzylidene)indolin-2-one (3b)

The title compound was obtained after silica (60–120 mesh) column chromatography (Hexane: Ethyl acetate: 85:15 to 70:30); Colour: Soft yellow needle; Yield: 98 %; MP: 198–200 °C; **^{1}H NMR** (500 MHz, $CDCl_3$) δ: 9.04 (s, 1H), 7.78 (s, 1H), 7.69–7.64 (m, 2H), 7.59 (d, J = 7.7 Hz, 1H), 7.22 (td, J = 7.7, 1.0 Hz, 1H), 7.19–7.14 (m, 2H), 6.94 (d, J = 7.7 Hz, 1H), 6.88 (td, J = 7.7, 1.0 Hz, 1H); **^{13}C NMR** (126 MHz, $CDCl_3$) δ: 170.53, 163.44 (d, J = 251.4 Hz), 141.91, 136.39, 131.55 (d, J = 8.1 Hz), 131.02 (d, J = 3.4 Hz), 130.17, 127.76, 122.97, 122.02, 121.66, 116.03 (d, J = 21.9 Hz), 110.57; **HR-MS** for $C_{15}H_{11}NOF$ $(M + H)^+$: 240.08, found: *m/z*: 240.08, 227.10, 203.05, 166.53.

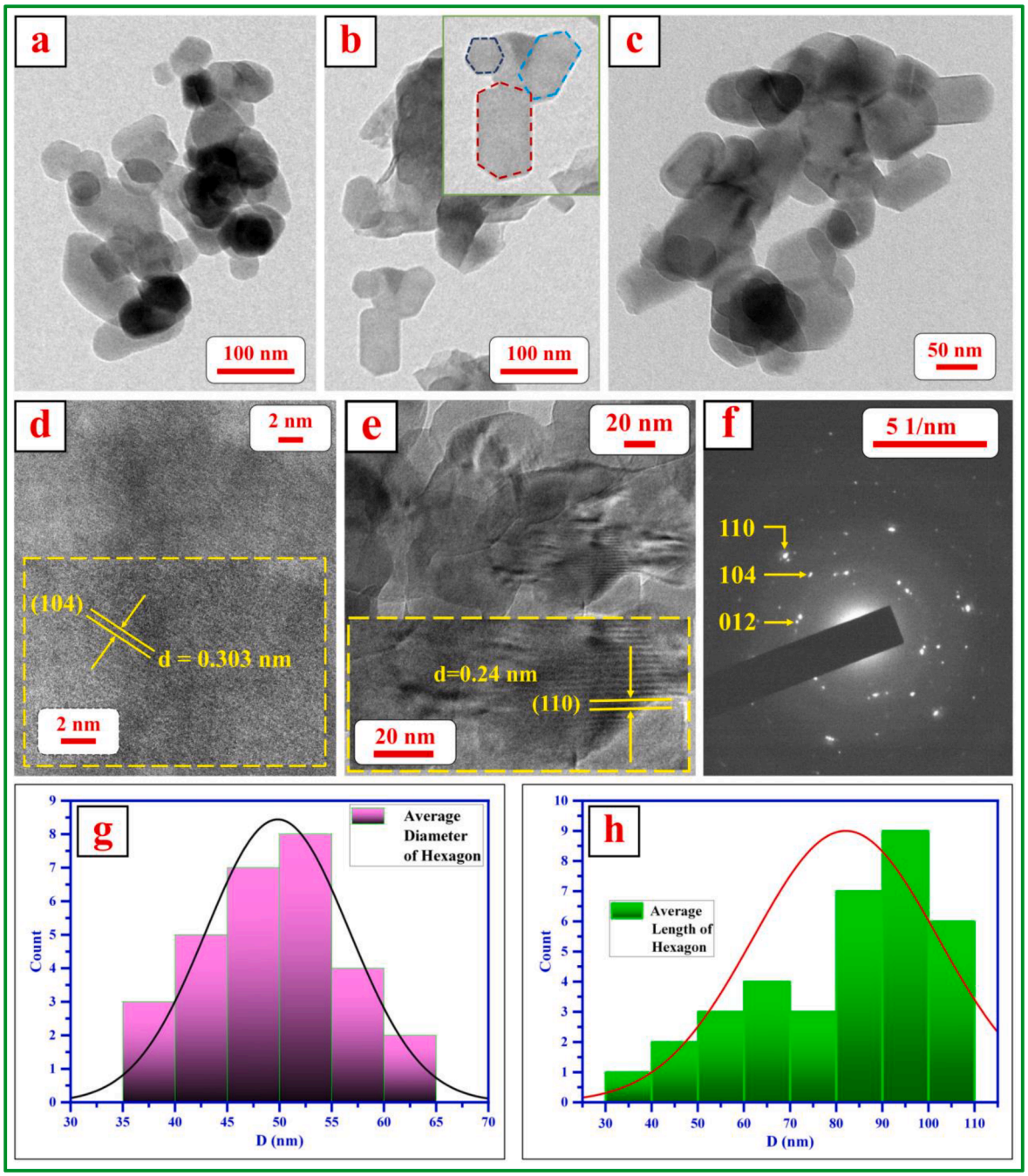

Fig. 5. HR-TEM images (a-f), histogram of the hexagon (g-h).

(E)-3-(4-chlorobenzylidene)indolin-2-one (3c)

The title compound was obtained after silica (60–120 mesh) column chromatography (Hexane: Ethyl acetate: 85:15 to 60:40); Colour: Soft yellow needle; Yield: 97 %; MP: 112–214 °C; **^{1}H NMR** (500 MHz, $CDCl_3$) δ: 8.96 (s, 1H), 7.76 (s, 1H), 7.60 (d, J = 8.1 Hz, 2H), 7.57 (d, J = 7.7 Hz, 1H), 7.45 (d, J = 8.1 Hz, 2H), 7.23 (t, J = 7.6 Hz, 1H), 6.93 (d, J = 7.7 Hz, 1H), 6.88 (t, J = 7.6 Hz, 1H); **^{13}C NMR** (126 MHz, $CDCl_3$) δ: 170.36, 141.96, 136.01, 135.71, 133.42, 130.79*, 130.34, 129.15*, 128.26, 123.14, 122.08, 121.57, 110.57; **HR-MS** for $C_{15}H_{11}NOCl$** $(M + H)^+$: 258.05, $C_{15}H_{11}NOCl$ $(M + H)^+$: 256.05, found: *m/z*: 227.10, 203.05, 174.52.

(E)-3-(4-bromobenzylidene)indolin-2-one (3d)

The title compound was obtained after silica (60–120 mesh) column chromatography (Hexane: Ethyl acetate: 95:5 to 50:50); Colour: Soft yellow needle; Yield: 98 %; MP: 254–256 °C; **^{1}H NMR** (500 MHz, $CDCl_3$) δ: 8.27 (s, 1H), 7.72 (s, 1H), 7.61 (d, J = 8.4 Hz, 2H), 7.57 (d, J = 7.5 Hz, 1H), 7.53 (d, J = 8.4 Hz, 2H), 7.23 (td, J = 7.7, 1.0 Hz, 1H), 6.91–6.86 (m, 2H); **^{13}C NMR** (126 MHz, $CDCl_3$) δ: 170.12, 141.85, 136.03, 133.88, 132.12*, 130.98*, 130.37, 128.23, 124.00, 123.19, 122.12, 121.58, 110.50; **HR-MS** for $C_{15}H_{11}NOBr$** $(M + H)^+$: 302.00, $C_{15}H_{11}NOBr$ $(M + H)^+$: 300.00, found: *m/z*: 302.00, 300.00, 294.94, 288.29, 284.91, 261.13, 243.94, 226.95, 217.11, 175.12, 158.96, 150.13, 135.00.

(E)-3-(2-fluorobenzylidene)indolin-2-one (3e)

The title compound was obtained after silica (60–120 mesh) column chromatography (Hexane: Ethyl acetate: 85:15 to 60:40); Colour: Bright yellow needle; Yield: 100 %; MP: 262–264 °C; **^{1}H NMR** (500 MHz, DMSO) δ: 10.63 (s, 1H), 7.73 (td, J = 7.6, 0.9 Hz, 1H), 7.56–7.50 (m, 2H), 7.34 (ddd, J = 7.5, 6.3, 4.8 Hz, 2H), 7.25 (d, J = 7.7 Hz, 1H), 7.22

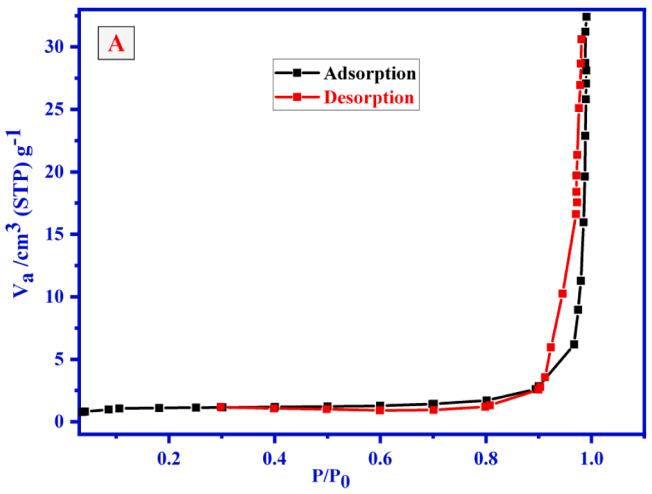

Fig. 6. Nitrogen adsorption-desorption isotherms at-196 °C (BET plot).

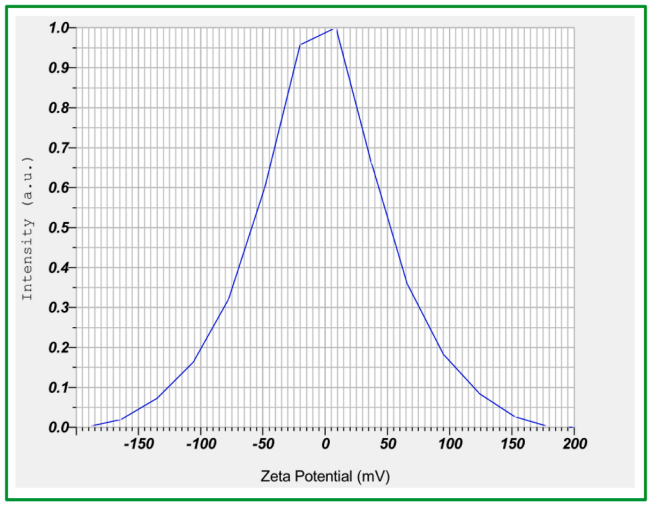

Fig. 7. Zeta potential distribution curve of synthesized $CaCO_3$ NFs.

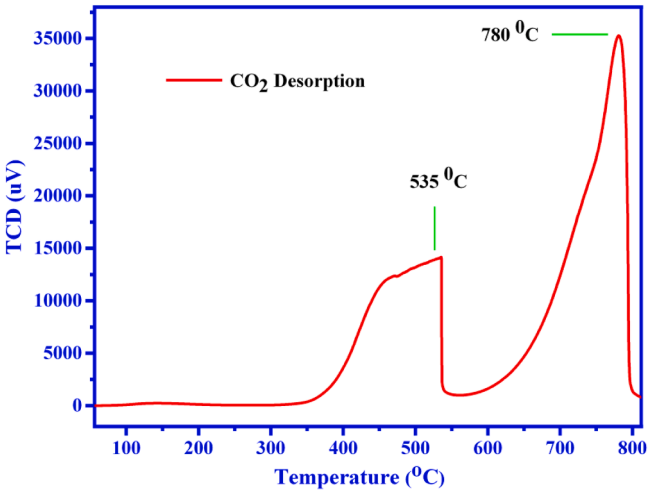

Fig. 8. The CO_2 adsorption-desorption curves for CO_2-TPD analysis on $CaCO_3$ NFs.

(td, J = 7.7, 1.0 Hz, 1H), 6.87 (d, J = 7.7 Hz, 1H), 6.82 (td, J = 7.6, 0.9 Hz, 1H); **^{13}C NMR** (126 MHz, DMSO) δ: 168.14, 159.72 (d, J = 248.8 Hz), 143.15, 131.88 (d, J = 8.2 Hz), 130.49, 130.41, 129.84, 127.36 (d, J = 2.8 Hz), 124.62 (d, J = 3.3 Hz), 122.67, 122.33 (d, J = 14.6 Hz), 121.23, 120.67, 116.01 (d, J = 20.8 Hz), 110.18; **HR-MS** for $C_{15}H_{11}NOF$ $(M + H)^+$: 240.08, found: *m/z*: 240.08, 227.10, 203.05.

(E)-3-(2-bromobenzylidene)indolin-2-one (3f)

The title compound was obtained after silica (60–120 mesh) column chromatography (Hexane: Ethyl acetate: 85:15 to 75:25); Colour: Bright yellow needle; Yield: 98 %; MP: 190–192 °C; **^{1}H NMR** (500 MHz, $CDCl_3$) δ: 9.01 (s, 1H), 7.82 (s, 1H), 7.71 (d, J = 8.3 Hz, 2H), 7.43–7.38 (m, 1H), 7.31 (dd, J = 7.8, 1.3 Hz, 1H), 7.28 (d, J = 8.3 Hz, 1H), 7.22 (td, J = 7.8, 0.8 Hz, 1H), 6.93 (d, J = 7.8 Hz, 1H), 6.81 (td, J = 7.6, 0.6 Hz, 1H); **^{13}C NMR** (126 MHz, $CDCl_3$) δ: 170.02, 142.05, 135.95, 135.60, 133.34, 130.97, 130.39*, 129.06, 127.39, 124.34, 123.35, 122.03, 121.51, 110.58; **HR-MS** for $C_{15}H_{11}NOBr$** $(M + H)^+$: 302.00, $C_{15}H_{11}NOBr$ $(M + H)^+$: 300.00, found: *m/z*: 302.00, 300.00, 266.11, 221.08, 203.05.

(E)-3-(4-hydroxybenzylidene)indolin-2-one (3g)

The title compound was obtained after silica (60–120 mesh) column chromatography (Hexane: Ethyl acetate: 85:15 to 40:60); Colour: Faint brown needle; Yield: 93 %; MP: 332–334 °C; **^{1}H NMR** (500 MHz, DMSO) δ: 10.50 (s, 1H), 10.17 (bs, 1H), 7.69 (d, J = 7.8 Hz, 1H), 7.60 (d, J = 8.5 Hz, 2H), 7.54 (s, 1H), 7.19 (td, J = 7.7, 1.0 Hz, 1H), 6.90 (d, J = 8.5 Hz, 2H), 6.87 (m, 2H); **^{13}C NMR** (126 MHz, DMSO) δ: 169.20, 159.36, 142.53, 136.70, 131.87*, 129.46, 125.09, 124.74, 122.10, 121.39, 121.09, 115.72*, 110.04; **HR-MS** for $C_{15}H_{12}NO_2$ $(M + H)^+$: 238.09, found: *m/z*: 238.09, 165.54.

(E)-3-(2-hydroxybenzylidene)indolin-2-one (3h)

The title compound was obtained after silica (60–120 mesh) column chromatography (Hexane: Ethyl acetate: 85:15 to 45:55); Colour: Bright yellow needle; Yield: 98 %; MP: 210–212 °C; **^{1}H NMR** (500 MHz, DMSO) δ: 10.49 (s, 1H), 10.12 (s, 1H), 7.70 (s, 1H), 7.61 (dd, J = 7.6, 1.2 Hz, 1H), 7.50 (d, J = 7.6 Hz, 1H), 7.28 (m, 1H), 7.17 (td, J = 7.7, 0.9 Hz, 1H), 6.97 (dd, J = 8.1, 0.5 Hz, 1H), 6.90 (t, J = 7.5 Hz, 1H), 6.85 (d, J = 7.7 Hz, 1H), 6.81 (td, J = 7.6, 0.9 Hz, 1H); **^{13}C NMR** (126 MHz, DMSO) δ: 168.89, 156.51, 142.61, 132.52, 131.47, 129.53, 129.47, 126.50, 122.33, 121.38, 121.35, 120.91, 118.74, 115.98, 109.92; **HR-MS** for $C_{15}H_{12}NO_2$ $(M + H)^+$: 238.09, found: *m/z*: 238.09, 227.10, 203.05, 165.54.

(E)-3-(4-methoxybenzylidene)indolin-2-one (3i)

The title compound was obtained after silica (60–120 mesh) column chromatography (Hexane: Ethyl acetate: 75:25 to 65:35); Colour: Faint yellow crystal; Yield: 95 %; MP: 192–194 °C; **^{1}H NMR** (500 MHz, $CDCl_3$) δ: 9.38 (s, 1H), 7.80 (s, 1H), 7.75 (d, J = 7.7 Hz, 1H), 7.68 (d, J = 8.7 Hz, 2H), 7.21 (td, J = 7.7, 0.7 Hz, 1H), 6.99 (d, J = 8.7 Hz, 2H), 6.95 (d, J = 7.7 Hz, 1H), 6.89 (td, J = 7.7, 0.7 Hz, 1H), 3.89 (s, 3H); **^{13}C NMR** (126 MHz, $CDCl_3$) δ: 171.15, 161.05, 141.73, 137.82, 131.66*, 129.56, 127.33, 125.94, 122.75, 122.10, 121.79, 114.23*, 110.47, 55.53; **HR-MS** for $C_{16}H_{14}NO_2$ $(M + H)^+$: 252.10, found: *m/z*: 252.10, 227.10, 203.05.

(E)-3-(2-methoxybenzylidene)indolin-2-one (3j)

The title compound was obtained after silica (60–120 mesh) column chromatography (Hexane: Ethyl acetate: 75:25 to 70:30); Colour: Faint yellow needle; Yield: 98 %; MP: 218–220 °C; **^{1}H NMR** (500 MHz, DMSO) δ: 10.57 (s, 1H), 7.67 (d, J = 1.4 Hz, 1H), 7.66 (s, 1H), 7.49–7.45 (m, 1H), 7.40 (d, J = 7.6 Hz, 1H), 7.20 (td, J = 7.7, 1.1 Hz, 1H), 7.14 (d, J = 8.0 Hz, 1H), 7.07 (t, J = 7.3 Hz, 1H), 6.87 (d, J = 7.7 Hz, 1H), 6.82 (td, J = 7.7, 1.1 Hz, 1H), 3.85 (s, 3H); **^{13}C NMR** (126 MHz, DMSO) δ: 168.69, 157.67, 142.76, 131.83, 131.79, 129.96, 129.55, 127.36, 122.86, 122.31, 121.13, 121.10, 120.27, 111.59, 110.10, 55.63; **HR-MS** for $C_{16}H_{14}NO_2$ $(M + H)^+$: 252.10, found: *m/z*: 252.10, 227.10.

(E)-3-(2,3,4-trimethoxybenzylidene)indolin-2-one (3k)

Table 1
Screening of catalysts for the C3-benzylidene-oxindole synthesis.

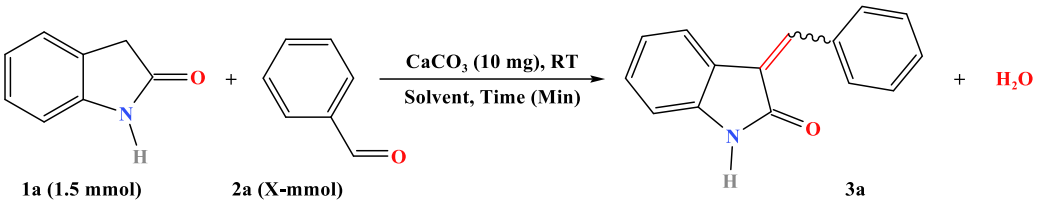

1a (1.5 mmol) 2a (X-mmol) 3a

Entry [a]	Catalyst	3a-Yield (%) [b]
1	Blank	No Reaction
2	K10 Montmorillonite	5
3	$CaCO_3$	11
4	Na_2CO_3	5
5	$Ca(NO_3)_2$	4
6	ZnO	17
7	NiO	15
8	CuO	24
9	MgO	37
10	CaO	59
11	**$CaCO_3$ NFs**	**74**

[a] Reaction Condition: 2-Oxindole (1.5 mmol), Benzaldehyde (1.8 mmol), Water:Ethanol (1:1) (2 mL), Catalyst (10 mg) at Room Temperature.
[b] Isolated yield.

Table 2
Screening of solvent and mole fraction of benzaldehyde for C3-benzylidene-oxindole synthesis.

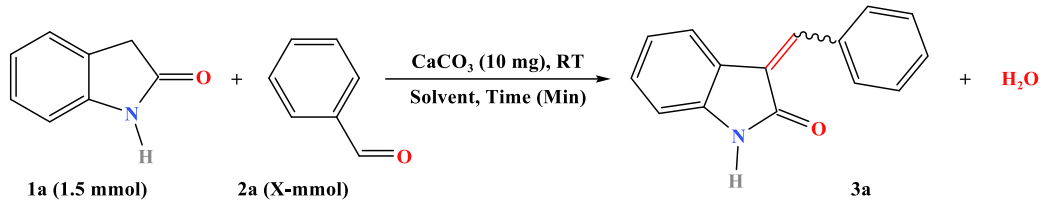

1a (1.5 mmol) 2a (X-mmol) 3a

Entry[a]	2a (X-mmol)	Solvent	Time (min)	3a-Yield (%)[b]
1	1.5	Water	30	65
2	1.5	Water: Ethanol (1:1)	25	69
3	1.5	Ethanol	90	51
4	1.5	Water: Methanol (1:1)	30	58
5	1.5	Methanol	90	42
6	1.5	DCM	60	4
7	1.5	Acetonitrile	60	11
8	1.5	1,4-Dioxane	60	8
9	1.5	Toluene	60	7
10	1.8	Water	30	72
11	**1.8**	**Water: Ethanol (1:1)**	**25**	**74**
12	1.8	Ethanol	90	59
13	1.8	Water: Methanol (1:1)	30	65
14	1.8	Methanol	90	52
15	2.0	Water	30	72
16	2.0	Water: Ethanol (1:1)	25	74
17	2.0	Ethanol	90	59
18	2.0	Water: Methanol (1:1)	30	65
19	2.0	Methanol	90	52

[a] Reaction Condition: 2-Oxindole (1.5 mmol), Benzaldehyde, Solvent (2 mL), Catalyst $CaCO_3$ NFs (0.1 mmol) at Room Temperature.
[b] Isolated yield.

The title compound was obtained after silica (60–120 mesh) column chromatography (Hexane: Ethyl acetate: 85:15 to 60:40); Colour: Bright yellow crystal; Yield: 96 %; MP: 256–258 °C; **^{1}H NMR** (500 MHz, $CDCl_3$) δ: 9.16 (s, 1H), 7.91 (s, 1H), 7.64 (d, J = 7.7 Hz, 1H), 7.51 (d, J = 8.7 Hz, 1H), 7.19 (t, J = 7.7 Hz, 1H), 6.94 (d, J = 7.7 Hz, 1H), 6.86 (t, J = 7.7 Hz, 1H), 6.74 (d, J = 8.7 Hz, 1H), 3.94 (s, 3H), 3.94 (s, 3H), 3.92 (s, 3H); **^{13}C NMR** (126 MHz, $CDCl_3$) δ: 170.75, 155.73, 153.44, 142.36, 141.69, 133.84, 129.54, 126.71, 124.98, 122.86, 122.18, 121.71, 121.69, 110.36, 106.96, 61.80, 61.14, 56.24; **HR-MS** for $C_{18}H_{18}NO_4$ $(M + H)^+$: 312.12, found: *m/z*: 312.12.

(E)-3-(2-nitrobenzylidene)indolin-2-one (3l)

The title compound was obtained after silica (60–120 mesh) column chromatography (Hexane: Ethyl acetate: 85:15 to 50:50); Colour: Faint yellow crystal; Yield: 94 %; MP: 256–258 °C; **^{1}H NMR** (500 MHz, DMSO) δ: 10.65 (s, 1H), 8.29 (dd, J = 7.5, 0.85 Hz, 1H), 7.87 (td, J = 7.5, 0.76 Hz, 1H), 7.82 (s, 1H), 7.79 (d, J = 7.5 Hz, 1H), 7.75 (td, J = 7.7, 1.0 Hz, 1H), 7.18 (td, J = 7.7, 1.0 Hz, 1H), 6.86 (d, J = 7.7 Hz, 1H), 6.79 (d, J = 7.5 Hz, 1H), 6.72 (td, J = 7.5, 0.69 Hz, 1H); **^{13}C NMR** (126 MHz, DMSO) δ: 168.10, 147.12, 143.10, 134.53, 132.41, 131.01, 130.70, 130.67, 130.49, 128.69, 125.25, 122.47, 121.28, 120.59, 110.38; **HR-MS** for $C_{15}H_{11}N_2O_3$ $(M + H)^+$: 267.08, found: *m/z*: 267.08, 249.07, 221.08, 203.05, 180.03, 132.04.

Table 3
Screening of catalytic amount for C3-benzylidene-oxindole synthesis.

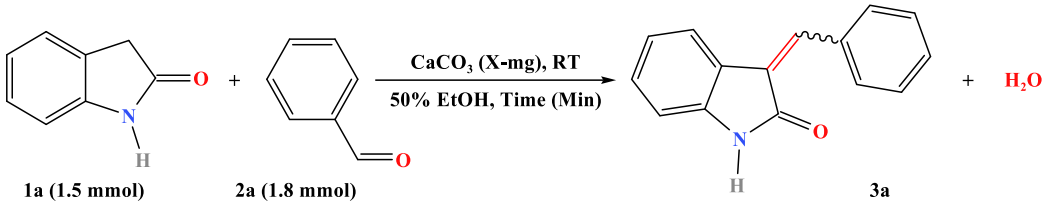

Entry[a]	Catalyst amount (mg)	Time (min)	3a-Yield (%)[b]
1	5	35	65
2	10	25	74
3	15	20	85
4	20	15	93
5	25	10	96
6	30	10	98*
7	**30**	**05**	**99**
8	35	05	99
9	40	05	99
10	45	05	99

[a] Reaction Condition: 2-Oxindoele (1.5 mmol), Benzaldehyde (1.8 mmol), Solvent (2 mL), Catalyst-$CaCO_3$ NFs at Room Temperature.
[b] Isolated yield.
[*] Water as a solvent.

Table 4
$CaCO_3$-catalyzed C3-arenylation of oxindole **(1a)** with aromatic aldehydes **(2a-2m)** to synthesize the corresponding 3-alkylidene-oxindoles **(3a-3m).**

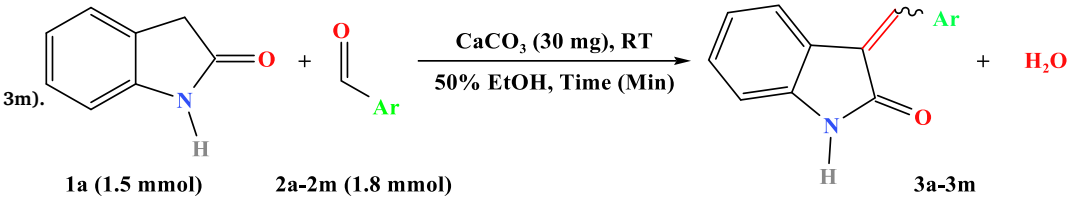

Entry	Aryl carbaldehyde	Product	Time (min)	Yield (%)[b]	TON	E:Z [c]	MP (°C)[d]	Ref.
1	Phenyl	**3a**	5	99	338.31	98:2	174–176	[2,6–9,11–12]
2	4-Fluoro Phenyl	**3b**	7	98	334.83	99:1	198–200	[2]
3	4-Chloro Phenyl	**3c**	7	97	331.44	99:1	212–214	[2,6–7,11–12]
4	4-Bromo Phenyl	**3d**	7	98	334.83	99:1	254–256	[6–7]
5	2-fluoro Phenyl	**3e**	7	98	334.83	100:0	262–264	[2]
6	2-Bromo Phenyl	**3f**	7	98	334.87	100:0	190–192	New
7	4-Hydroxy Phenyl	**3g**	17	93	317.80	93:7	332–334	[11]
8	2-Hydroxy Phenyl	**3h**	9	98	334.81	92:8	210–212	[7,12]
9	4-Methoxy Phenyl	**3i**	18	94	321.15	100:0	192–194	[2,6–7,11–12]
10	2-Methoxy Phenyl	**3j**	8	98	334.82	100:0	218–220	[2,11]
11	2, 3, 4-Tri Methoxy Phenyl	**3k**	9	96	327.98	98:2	172–174	New
12	2-Nitro Phenyl	**3l**	7	94	321.15	99:1	256–258	[6–7]
13	2-Hydroxy Naphthalene 1-yl	**3m**	10	98	334.82	96:4	340–342	New

[b] Isolable yield.
[c] Ratio of E/Z isomers after column chromatography.
[d] Physical constant of major isomer.

Table 5
Comparative study of Knoevenagel reaction with previous reports.

Oxindole		Substrate (2a)		Catalyst		Solvent	Temp. °C	Time	Yield %	Ref.
R1	Loading	Aldehyde / alcohol	Loading	Catalyst	loading					
Phenyl	0.2 mmol	Benzyl alcohol	0.8 mmol	$ReH_7(PCy_3)_2$	5 mol %	anisole	150 °C	36 h	75	[51]
H	1 mmol	Benzaldehyde	1 mmol	UiO-66	30 mg	dodecane	80 °C	2 h	80	[53]
H	1 mmol	Benzaldehyde	1 mmol	$[(CH_2)_3SO_3Hmim]HSO_4$	2 mL	–	80 °C	1 h	93	[55]
H	3 mmol	Benzaldehyde	3 mmol	$KF\text{-}Al_2O_3$	3 gm	Acetonitrile	–	3 min	94	[56]
H	0.3 mmol	Benzaldehyde	1.2 eq.	Ti $(O^iPr)_4$	0.8 eq.	THF	RT	3 h	92 (E:79 %)	[57]
H	1 mmol	Benzaldehyde	1 mmol	$SBA\text{-}Pr\text{-}SO_3H$	20 mg	Solvent Free	120 °C	0.5 h	90	[59]
H	1 mmol	Benzaldehyde	1.25 mmol	CeO_2	20 mg	Solvent Free	100 °C	10 h	85 (E:88 %)	[60]
H	**1 mmol**	**Benzaldehyde**	**1.2 mmol**	**$CaCO_3$**	**0.027 mmol**	**Water: Ethanol (1:1)**	**RT**	**5 min**	**98 (E:98 %)**	**Present Work**

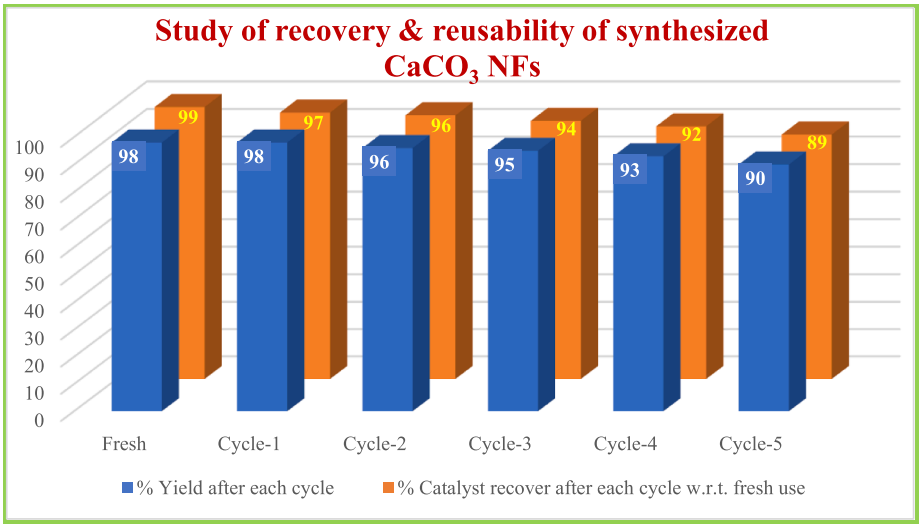

Fig. 9. $CaCO_3$ nanoflower catalyst recovery and reuse for the synthesis of C3-arenyl oxindoles from 1a and 2a under standard conditions shown in Table 5 (Entry 1).

(E)-3-((2-hydroxynaphthalen-1-yl)methylene)indolin-2-one (3m)

The title compound was obtained after silica (60–120 mesh) column chromatography (Hexane: Ethyl acetate: 85:15 to 30:70); Colour: Bright brown crystal; Yield: 98 %; MP: 340–342 °C; **^{1}H NMR** (500 MHz, DMSO) δ: 10.70 (s, 1H), 10.35 (bs, 1H), 8.63 (s, 1H), 8.46 (d, J = 7.7 Hz, 1H), 8.07 (dd, J = 7.6, 1.1 Hz, 1H), 7.66–7.56 (m, 5H), 7.14 (t, J = 7.6 Hz, 1H), 6.81 (d, J = 7.7 Hz, 1H), 6.73 (t, J = 7.7 Hz, 1H); **^{13}C NMR** (126 MHz, DMSO) δ: 171.94, 169.51, 151.55, 142.46, 140.85, 133.34, 131.41, 131.04*, 130.77, 130.72, 129.12, 126.36, 125.65, 123.85, 122.79, 120.65, 114.49, 110.18; **HR-MS** for $C_{19}H_{14}NO_2$ $(M + H)^+$: 288.10, found: *m/z*: 288.10, 276.07, 262.09, 250.18, 226.95, 212.05, 200.54, 191.53, 180.02, 162.01, 149.02, 124.09, 101.07, 90.98.

[**Note**- a) * Indicates chemical shift for two chemically and magnetically equivalent carbons in molecule for ^{13}C NMR. b) ** Indicate the *m/z* peak position of the Isotopic peak of the halogen atom present in the product molecule for HR-MS].

3.2. Study of recovery and reusability of synthesized $CaCO_3$ NFs

After completing the reaction process, separated Calcite nanoparticles ($CaCO_3$ NFs) were washed five to six times with ethyl acetate, then dried in an oven at 100 °C for 3 h, activating the same NFs in a muffle furnace at 250 °C for 3 h after every reuse. Before and after reuse six times, the characterization of the Calcite nanoparticles ($CaCO_3$ NFs) showed the same morphology and particle size by the FE-SEM image. Interestingly, the catalytic activity and reusability of the $CaCO_3$ nanoflowers were not affected when it was reused numerous times. The corresponding yield for each cycle is mentioned in the graphical chart Fig. 9**.** This is the first time we have used a $CaCO_3$ catalyst in Knoevenagel synthesis.

4. Conclusion

In the present study, a heterogeneous Calcite nanoflowers catalyst was found to be a highly efficient catalyst for the synthesis of specifically *E*-3-arylidene-2-oxindole using 2-oxindole and aromatic aldehyde. Catalytic synthesis of 3-arylidene-2-oxindole is highly affected by solvent polarity, and it was studied by using nine non-polar to polar organic solvents and found that the conversion of 2-oxindole percentage was increased with solvent polarity. This is due to increasing the Lewis acid-base interaction between the catalysts and 2-oxindole in the presence of the polar protic solvent. Furthermore, the morphological study of catalysts suggests that the defect-free $CaCO_3$ most stable (1 0 4) surface is an active site for the arenylation of 2-oxindole.

CRediT authorship contribution statement

Dnyaneshwar Sanap: Data curation, Writing – original draft. **Lata Avhad:** Data curation, Visualization, Investigation. **Suresh Ghotekar:** Data curation, Visualization, Investigation, Writing – review & editing. **Nitin D. Gaikwad:** Data curation, Visualization, Writing – review & editing.

Declaration of Competing Interest

The authors declare that they have no known competing financial interests or personal relationships that could have appeared to influence the work reported in this paper.

Data availability

Data will be made available on request.

Acknowledgments

The authors acknowledge Central Instrumentation Facilities (CIF), Savitribai Phule Pune University (SPPU), Pune, for UV-DRS, IR, BET, XRD, FE-SEM, and HR-MS analysis. We thank STIC, Cochin University, Kerala, for the HR-TEM analysis. The authors also thank the Sophisticated Analytical Instrumentation Facility (SAIF) for ^{1}H and ^{13}C FT-NMR.

Funding

This study was financially supported by the University Grant Commission (UGC), Government of India, India, File No: F.47-1129/14 (General/4/WRO)XII Plan.

References

[1] Y.M. Khetmalis, et al., Oxindole and its derivatives: A review on recent progress in biological activities, Biomed. Pharmacother. 141 (2021), 111842.
[2] A. Millemaggi, R.J. Taylor, 3-Alkenyl-oxindoles: Natural Products, Pharmaceuticals, and Recent Synthetic Advances in Tandem/Telescoped Approaches, Eur. J. Org. Chem. 2010 (24) (2010) 4527–4547.
[3] M. Kaur, M. Singh, N. Chadha, O.m. Silakari, Oxindole: A chemical prism carrying plethora of therapeutic benefits, Eur. J. Med. Chem. 123 (2016) 858–894.
[4] P. Chaudhari, et al., Logical synthetic strategies and structure-activity relationship of indolin-2-one hybrids as small molecule anticancer agents: An overview, J. Mol. Struct. 1247 (2022), 131280.
[5] L.-M. Zhou, R.-Y. Qu, G.-F. Yang, An overview of spirooxindole as a promising scaffold for novel drug discovery, Expert Opin. Drug Discov. 15 (5) (2020) 603–625.

[6] Y. Zheng, C.M. Tice, S.B. Singh, The use of spirocyclic scaffolds in drug discovery, Bioorg. Med. Chem. Lett. 24 (16) (2014) 3673–3682.
[7] R. Dalpozzo, Catalytic asymmetric synthesis of hetero-substituted oxindoles, Org. Chem. Front. 4 (10) (2017) 2063–2078.
[8] P. Chauhan, S.S. Chimni, Organocatalytic asymmetric synthesis of 3-amino-2-oxindole derivatives bearing a tetra-substituted stereocenter. Tetrahedron: Asymmetry, 2013. **24**(7): p. 343-356.
[9] R.A. Blake, M.A. Broome, X. Liu, J. Wu, M. Gishizky, L.i. Sun, S.A. Courtneidge, SU6656, a selective src family kinase inhibitor, used to probe growth factor signaling, Mol. Cell. Biol. 20 (23) (2000) 9018–9027.
[10] L.i. Sun, N. Tran, C. Liang, F. Tang, A. Rice, R. Schreck, K. Waltz, L.K. Shawver, G. McMahon, C. Tang, Design, synthesis, and evaluations of substituted 3-[(3-or 4-carboxyethylpyrrol-2-yl) methylidenyl] indolin-2-ones as inhibitors of VEGF, FGF, and PDGF receptor tyrosine kinases, J. Med. Chem. 42 (25) (1999) 5120–5130.
[11] L.i. Sun, C. Liang, S. Shirazian, Y. Zhou, T. Miller, J. Cui, J.Y. Fukuda, J.-Y. Chu, A. Nematalla, X. Wang, H. Chen, A. Sistla, T.C. Luu, F. Tang, J. Wei, C. Tang, Discovery of 5-[5-fluoro-2-oxo-1, 2-dihydroindol-(3 Z)-ylidenemethyl]-2, 4-dimethyl-1 H-pyrrole-3-carboxylic acid (2-diethylaminoethyl) amide, a novel tyrosine kinase inhibitor targeting vascular endothelial and platelet-derived growth factor receptor tyrosine kinase, J. Med. Chem. 46 (7) (2003) 1116–1119.
[12] L. Sun, N. Tran, C. Liang, S. Hubbard, F. Tang, K. Lipson, R. Schreck, Y. Zhou, G. McMahon, C. Tang, Identification of substituted 3-[(4, 5, 6, 7-tetrahydro-1 H-indol-2-yl) methylene]-1, 3-dihydroindol-2-ones as growth factor receptor inhibitors for VEGF-R2 (Flk-1/KDR), FGF-R1, and PDGF-Rβ tyrosine kinases, J. Med. Chem. 43 (14) (2000) 2655–2663.
[13] J. Caballero, et al., Synthesis, in silico, in vitro, and in vivo investigation of 5-[11C] methoxy-substituted sunitinib, a tyrosine kinase inhibitor of VEGFR-2, Eur. J. Med. Chem. 58 (2012) 272–280.
[14] R.R. Khanwelkar, G.S. Chen, H.-C. Wang, C.-W. Yu, C.-H. Huang, O.n. Lee, C.-H. Chen, C.-S. Hwang, C.-H. Ko, N.-T. Chou, M.-W. Lin, L.-M. Wang, Y.-C. Chen, T.-H. Hseu, C.-N. Chang, H.-C. Hsu, H.-C. Lin, Y.-C. Shih, S.-H. Chou, H.-W. Tseng, C.-P. Liu, C.-M. Tu, T.-L. Hu, Y.-J. Tsai, J.-W. Chern, Synthesis and structure–activity relationship of 6-arylureido-3-pyrrol-2-ylmethylideneindolin-2-one derivatives as potent receptor tyrosine kinase inhibitors, Bioorg. Med. Chem. 18 (13) (2010) 4674–4686.
[15] H.K. Ho, B.T. Chua, W. Wong, K.S. Lim, V. Teo, H.-T. Ong, X. Chen, W. Zhang, K. M. Hui, M.L. Go, A. Ullrich, Benzylidene-indolinones are effective as multi-targeted kinase inhibitor therapeutics against hepatocellular carcinoma, Mol. Oncol. 8 (7) (2014) 1266–1277.
[16] D. Bensinger, D. Stubba, A. Cremer, V. Kohl, T. Waßmer, J. Stuckert, V. Engemann, K. Stegmaier, K. Schmitz, B. Schmidt, Virtual screening identifies irreversible FMS-like tyrosine kinase 3 inhibitors with activity toward resistance-conferring mutations, J. Med. Chem. 62 (5) (2019) 2428–2446.
[17] A. Andreani, S. Burnelli, M. Granaiola, A. Leoni, A. Locatelli, R. Morigi, M. Rambaldi, L. Varoli, M.W. Kunkel, Antitumor activity of substituted E-3-(3, 4, 5-trimethoxybenzylidene)-1, 3-dihydroindol-2-ones, J. Med. Chem. 49 (23) (2006) 6922–6924.
[18] B. Pandit, Y. Sun, P. Chen, D.L. Sackett, Z. Hu, W. Rich, C. Li, A. Lewis, K. Schaefer, P.-K. Li, Structure–activity-relationship studies of conformationally restricted analogs of combretastatin A-4 derived from SU5416, Bioorg. Med. Chem. 14 (19) (2006) 6492–6501.
[19] A. Nagarsenkar, et al., Synthesis and apoptosis inducing studies of triazole linked 3-benzylidene isatin derivatives, Eur. J. Med. Chem. 124 (2016) 782–793.
[20] K.R. Senwar, T.S. Reddy, D. Thummuri, P. Sharma, V.G.M. Naidu, G. Srinivasulu, N. Shankaraiah, Design, synthesis and apoptosis inducing effect of novel (Z)-3-(3′-methoxy-4′-(2-amino-2-oxoethoxy)-benzylidene) indolin-2-ones as potential antitumour agents, Eur. J. Med. Chem. 118 (2016) 34–46.
[21] Y. Lai, L. Ma, W. Huang, X. Yu, Y. Zhang, H. Ji, J. Tian, Synthesis and biological evaluation of 3-[4-(amino/methylsulfonyl) phenyl] methylene-indolin-2-one derivatives as novel COX-1/2 and 5-LOX inhibitors, Bioorg. Med. Chem. Lett. 20 (24) (2010) 7349–7353.
[22] W. Zhang, M.-L. Go, Functionalized 3-benzylidene-indolin-2-ones: Inducers of NAD (P) H-quinone oxidoreductase 1 (NQO1) with antiproliferative activity, Bioorg. Med. Chem. 17 (5) (2009) 2077–2090.
[23] A.S. Girgis, et al., 3-Alkenyl-2-oxindoles: Synthesis, antiproliferative and antiviral properties against SARS-CoV-2, Bioorg. Chem. 114 (2021), 105131.
[24] M. Balderamos, H. Ankati, S.K. Akubathini, A.V. Patel, S. Kamila, C. Mukherjee, L. Wang, E.R. Biehl, S.R. D'Mello, Synthesis and structure-activity relationship studies of 3-substituted indolin-2-ones as effective neuroprotective agents, Exp. Biol. Med. 233 (11) (2008) 1395–1402.
[25] H. Watanabe, M. Ono, H. Kimura, K. Matsumura, M. Yoshimura, Y. Okamoto, M. Ihara, R. Takahashi, H. Saji, Synthesis and biological evaluation of novel oxindole derivatives for imaging neurofibrillary tangles in Alzheimer's disease, Bioorg. Med. Chem. Lett. 22 (17) (2012) 5700–5703.
[26] A. Luczywo, L.G. González, A.C.C. Aguiar, J. Oliveira de Souza, G.E. Souza, G. Oliva, L.F. Aguilar, J.J. Casal, R.V.C. Guido, S.E. Asís, M. Mellado, 3-aryl-indolinones derivatives as antiplasmodial agents: synthesis, biological activity and computational analysis, Nat. Prod. Res. 36 (15) (2022) 3887–3893.
[27] S.K. Suthar, S. Bansal, M.M. Alam, V. Jaiswal, A. Tiwari, A. Chaudhary, A.T. Alex, A. Joseph, Design, synthesis, and biological evaluation of oxindole derivatives as antidepressive agents, Bioorg. Med. Chem. Lett. 25 (22) (2015) 5281–5285.
[28] C.L. Woodard, Z. Li, A.K. Kathcart, J. Terrell, L. Gerena, M. Lopez-Sanchez, D. E. Kyle, A.K. Bhattacharjee, D.A. Nichols, W. Ellis, S.T. Prigge, J.A. Geyer, N. C. Waters, Oxindole-Based Compounds Are Selective Inhibitors of Plasmodium f alciparum Cyclin Dependent Protein Kinases, J. Med. Chem. 46 (18) (2003) 3877–3882.
[29] N.R. Ball-Jones, J.J. Badillo, A.K. Franz, Strategies for the enantioselective synthesis of spirooxindoles, Org. Biomol. Chem. 10 (27) (2012) 5165–5181.
[30] L. Hong, R. Wang, Recent Advances in Asymmetric Organocatalytic Construction of 3, 3′-Spirocyclic Oxindoles, Adv. Synth. Catal. 355 (6) (2013) 1023–1052.
[31] A.J. Boddy, J.A. Bull, Stereoselective synthesis and applications of spirocyclic oxindoles, Org. Chem. Front. 8 (5) (2021) 1026–1084.
[32] A.P. Sakla, P. Kansal, N. Shankaraiah, Syntheses and applications of spirocyclopropyl oxindoles: a decade review, Eur. J. Org. Chem. 2021 (5) (2021) 757–772.
[33] G. Molteni, A. Silvani, Spiro-2-oxindoles via 1, 3-dipolar cycloadditions. A decade update, Eur. J. Org. Chem. 2021 (11) (2021) 1653–1675.
[34] X.-H. Chen, Q. Wei, S.-W. Luo, H. Xiao, L.-Z. Gong, Organocatalytic synthesis of spiro [pyrrolidin-3, 3′-oxindoles] with high enantiopurity and structural diversity, J. Am. Chem. Soc. 131 (38) (2009) 13819–13825.
[35] B.M. Trost, N. Cramer, S.M. Silverman, Enantioselective construction of spirocyclic oxindolic cyclopentanes by palladium-catalyzed trimethylenemethane-[3+ 2]-cycloaddition, J. Am. Chem. Soc. 129 (41) (2007) 12396–12397.
[36] J. Liu, H. Sun, X. Liu, L. Ouyang, T. Kang, Y. Xie, X. Wang, Direct construction of novel exo′-selective spiropyrrolidine bisoxindoles via a three-component 1, 3-dipolar cycloaddition reaction, Tetrahedron Lett. 53 (18) (2012) 2336–2340.
[37] X.-F. Huang, Z.-M. Liu, Z.-C. Geng, S.-Y. Zhang, Y. Wang, X.-W. Wang, Enantioselective construction of multifunctionalized spirocyclohexaneoxindoles through organocatalytic Michael-Aldol cyclization of isatin derived alkenes with linear dialdehydes, Org. Biomol. Chem. 10 (44) (2012) 8794.
[38] D. Ramachary, C. Venkaiah, P.M. Krishna, Stereoselective synthesis of five-membered spirooxindoles through Tomita zipper cyclization, Org. Lett. 15 (18) (2013) 4714–4717.
[39] B. Viswambharan, K. Selvakumar, S. Madhavan, P. Shanmugam, Pyridine Core Activation via 1, 5-Electrocyclization of Vinyl Pyridinium Ylides Generated from Bromo Isomerized Morita− Baylis− Hillman Adduct of Isatin and Pyridine: Synthesis of 3-Spirodihydroindolizine Oxindoles, Org. Lett. 12 (9) (2010) 2108–2111.
[40] S. Lin, Z.-Q. Yang, B.H.B. Kwok, M. Koldobskiy, C.M. Crews, S.J. Danishefsky, Total synthesis of TMC-95A and-B via a new reaction leading to Z-enamides. Some preliminary findings as to SAR, J. Am. Chem. Soc. 126 (20) (2004) 6347–6355.
[41] T. Fukuyama, G. Liu, Stereocontrolled total synthesis of (±)-gelsemine, J. Am. Chem. Soc. 118 (31) (1996) 7426–7427.
[42] T. Jiang, K.L. Kuhen, K. Wolff, H. Yin, K. Bieza, J. Caldwell, B. Bursulaya, T. Tuntland, K. Zhang, D. Karanewsky, Y. He, Design, synthesis, and biological evaluations of novel oxindoles as HIV-1 non-nucleoside reverse transcriptase inhibitors. Part 2, Bioorg. Med. Chem. Lett. 16 (8) (2006) 2109–2112.
[43] T. Jiang, K.L. Kuhen, K. Wolff, H. Yin, K. Bieza, J. Caldwell, B. Bursulaya, T.-H. Wu, Y. He, Design, synthesis and biological evaluations of novel oxindoles as HIV-1 non-nucleoside reverse transcriptase inhibitors. Part I. Bioorg. Med. Chem. Lett. 16 (8) (2006) 2105–2108.
[44] B. Yu, Z. Yu, P.-P. Qi, D.-Q. Yu, H.-M. Liu, Discovery of orally active anticancer candidate CFI-400945 derived from biologically promising spirooxindoles: Success and challenges, Eur. J. Med. Chem. 95 (2015) 35–40.
[45] B. Yu, Y.-C. Zheng, X.-J. Shi, P.-P. Qi, H.-M. Liu, Natural Product-Derived Spirooxindole Fragments Serve as Privileged Substructures for Discovery of New Anticancer Agents, ACAMC 16 (10) (2016) 1315–1324.
[46] A.M. Al-Majid, M. Ali, M.S. Islam, S. Alshahrani, A.S. Alamary, S. Yousuf, M. I. Choudhary, A. Barakat, Stereoselective Synthesis of the Di-Spirooxindole Analogs Based Oxindole and Cyclohexanone Moieties as Potential Anticancer Agents, Molecules 26 (20) (2021) 6305.
[47] V.R. Shah, J.D. Bhaliya, G.M. Patel, In silico approach: docking study of oxindole derivatives against the main protease of COVID-19 and its comparison with existing therapeutic agents, J. Basic Clin. Physiol. Pharmacol. 32 (3) (2021) 197–214.
[48] K. Acosta-Quiroga, C. Rojas-Peña, L.S. Nerio, M. Gutiérrez, E. Polo-Cuadrado, Spirocyclic derivatives as antioxidants: a review, RSC Adv. 11 (36) (2021) 21926–21954.
[49] L. Sun, et al., Synthesis and biological evaluations of 3-substituted indolin-2-ones: a novel class of tyrosine kinase inhibitors that exhibit selectivity toward particular receptor tyrosine kinases, J. Med. Chem. 41 (14) (1998) 2588–2603.
[50] A. Nagarsenkar, S.K. Prajapti, S.D. Guggilapu, S. Birineni, S. Sravanti Kotapalli, R. Ummanni, B.N. Babu, Investigation of triazole-linked indole and oxindole glycoconjugates as potential anticancer agents: novel Akt/PKB signaling pathway inhibitors, MedChemComm 7 (4) (2016) 646–653.
[51] H. Jin, J. Xie, C. Pan, Z. Zhu, Y. Cheng, C. Zhu, Rhenium-catalyzed acceptorless dehydrogenative coupling via dual activation of alcohols and carbonyl compounds, ACS Catal. 3 (10) (2013) 2195–2198.
[52] A. Kanyal, et al., *Ru-Catalyzed dehydrogenative synthesis of antimalarial arylidene oxindoles.* 2018.
[53] C. Van Goethem, M. Mertens, F.G. Cirujano, J.W. Seo, D. De Vos, I.F. J. Vankelecom, Improved MOF nanoparticle recovery and purification using crosslinked PVDF membranes, Chem. Commun. 54 (53) (2018) 7370–7373.
[54] Y. Ding, X. Xiang, M. Gu, H. Xu, H.e. Huang, Y.i. Hu, Efficient lipase-catalyzed Knoevenagel condensation: utilization of biocatalytic promiscuity for synthesis of benzylidene-indolin-2-ones, Bioprocess Biosyst. Eng. 39 (1) (2016) 125–131.
[55] Y.i. Hu, H. Kang, B.-W. Zeng, P. Wei, H.e. Huang, Facile synthesis of 3-arylidene-1, 3-dihydroindol-2-ones catalysed by a Brønsted acidic ionic liquid, J. Chem. Res. 2008 (11) (2008) 642–643.
[56] D. Villemin, B. Martin, Potassium fluoride on alumina: dry synthesis of 3-arylidene-1, 3-dihydro-indol-2-one under microwave irradiation, Synth. Commun. 28 (17) (1998) 3201–3208.

[57] H.J. Lee, et al., An expedient synthesis of 3-alkylideneoxindoles by Ti (OiPr) 4/pyridine-mediated Knoevenagel condensation, Tetrahedron Lett. 55 (6) (2014) 1183–1187.
[58] P. Gholamzadeh, G. Mohammadi Ziarani, A. Badiei, A. Abolhassani Soorki, N. Lashgari, Efficient green synthesis of isoindigo derivatives using sulfonic-acid-functionalized nanoporous silica (SBA-Pr-SO3H) catalyst and study of their antimicrobial properties, Res. Chem. Intermed. 39 (9) (2013) 3925–3936.
[59] P. Gholamzadeh, G.M. Ziarani, A. Badiei, Z. Bahrami, Application of sulfonic acid functionalized nanoporous silica (SBA-Pr-SO3H) in the solvent free synthesis of (E)-arylidene-1, 3-dihydroindole-2-ones, Eur. J. Chem. 3 (3) (2012) 279–282.
[60] M.N. Rashed, A.S. Touchy, C. Chaudhari, J. Jeon, S.M.A.H. Siddiki, T. Toyao, K.-I. Shimizu, Selective C3-alkenylation of oxindole with aldehydes using heterogeneous CeO2 catalyst, Chin. J. Catal. 41 (6) (2020) 970–976.
[61] A. Ghadami Jadval Ghadam, M. Idrees, Characterization of CaCO3 nanoparticles synthesized by reverse microemulsion technique in different concentrations of surfactants, Iran. J. Chem. Chem. Eng. (IJCCE), **32**(3) (2013) 27-35.
[62] A. Samanta, D.K. Chanda, P.S. Das, J. Ghosh, A. Dey, S. Das, A.K. Mukhopadhyay, Synthesis of mixed calcite–calcium oxide nanojasmine flowers, Ceram. Int. 42 (2) (2016) 2339–2348.
[63] A. Roy, J. Bhattacharya, Microwave-assisted synthesis and characterization of CaO nanoparticles, Int. J. Nanosci. 10 (03) (2011) 413–418.
[64] R.G. Jalu, T.A. Chamada, R. Kasirajan, Calcium oxide nanoparticles synthesis from hen eggshells for removal of lead (Pb (II)) from aqueous solution, Environ. Challenges 4 (2021), 100193.
[65] T. Liu, Y. Zhu, X. Zhang, T. Zhang, T. Zhang, X. Li, Synthesis and characterization of calcium hydroxide nanoparticles by hydrogen plasma-metal reaction method, Mater. Lett. 64 (23) (2010) 2575–2577.
[66] S. Gunasekaran, G. Anbalagan, Spectroscopic study of phase transitions in natural calcite mineral, Spectrochim. Acta A Mol. Biomol. Spectrosc. 69 (4) (2008) 1246–1251.
[67] V. Ramasamy, P. Anand, G. Suresh, Synthesis and characterization of polymer-mediated CaCO3 nanoparticles using limestone: a novel approach, Adv. Powder Technol. 29 (3) (2018) 818–834.
[68] M. Kosmulski, pH-dependent surface charging and points of zero charge. IV. Update and new approach, J. Colloid Interface Sci. 337 (2) (2009) 439–448.
[69] E. Ulkeryildiz, S. Kilic, E. Ozdemir, Rice-like hollow nano-CaCO3 synthesis, J. Cryst. Growth 450 (2016) 174–180.